



City Research Online

City, University of London Institutional Repository

Citation: Spieser, L., Kohl, C., Forster, B., Bestmann, S. & Yarrow, K. (2018). Neurodynamic Evidence Supports a Forced-Excursion Model of Decision-Making under Speed/Accuracy Instructions. eNeuro, doi: 10.1523/ENEURO.0159-18.2018

This is the accepted version of the paper.

This version of the publication may differ from the final published version.

Permanent repository link: <http://openaccess.city.ac.uk/19866/>

Link to published version: <http://dx.doi.org/10.1523/ENEURO.0159-18.2018>

Copyright and reuse: City Research Online aims to make research outputs of City, University of London available to a wider audience. Copyright and Moral Rights remain with the author(s) and/or copyright holders. URLs from City Research Online may be freely distributed and linked to.

City Research Online:

<http://openaccess.city.ac.uk/>

publications@city.ac.uk

Research Article: New Research / Cognition and Behavior

Neurodynamic Evidence Supports a Forced-Excursion Model of Decision-Making under Speed/Accuracy Instructions

Laure Spieser¹, Carmen Kohl¹, Bettina Forster¹, Sven Bestmann² and Kielan Yarrow¹

¹Department of Psychology, Cognitive Neuroscience Research Unit, University of London, London, EC1V 0HB, UK

²Sobell Department of Motor Neuroscience and Movement Disorders, UCL Institute of Neurology, University College London, London, WC1N 3BG, UK

DOI: 10.1523/ENEURO.0159-18.2018

Received: 23 April 2018

Accepted: 8 May 2018

Published: 4 June 2018

Author Contributions: K.Y., B.F. and S.B conceived the research programme. C.K., L.S. and K.Y. designed the experiment; C.K. and L.S. conducted the research and analysed the data; C.K. drafted the paper, which all authors critically revised and approved.

Funding: <http://doi.org/10.13039/501100000275>Leverhulme Trust RPG-2014188

Conflict of Interest: Authors declare no conflict of interest.

This work was funded by a Leverhulme Trust Research Project Grant (RPG-2014188).

LS and CK are contributed equally to this work.

Correspondence: Carmen Kohl, City University of London, Rhind Building, EC1V 0HB, London. E-mail: carmen.kohl@city.ac.uk

Cite as: eNeuro 2018; 10.1523/ENEURO.0159-18.2018

Alerts: Sign up at eneuro.org/alerts to receive customized email alerts when the fully formatted version of this article is published.

Accepted manuscripts are peer-reviewed but have not been through the copyediting, formatting, or proofreading process.

Copyright © 2018 Spieser et al.

This is an open-access article distributed under the terms of the Creative Commons Attribution 4.0 International license, which permits unrestricted use, distribution and reproduction in any medium provided that the original work is properly attributed.

Neurodynamic Evidence Supports a Forced-Excursion Model of Decision-Making under Speed/Accuracy Instructions

Abbreviated title: Neural signals support forced-excursion SAT model

Laure Spieser^{1,2}, Carmen Kohl^{1,2}, Bettina Forster², Sven Bestmann³, Kielan Yarrow²

¹ These authors contributed equally

Author Affiliations:

² Department of Psychology, Cognitive Neuroscience Research Unit,
City, University of London, EC1V 0HB, UK

³ Sobell Department of Motor Neuroscience and Movement Disorders, UCL Institute of
Neurology, University College London, WC1N 3BG, UK

Author Contributions: K.Y., B.F. and S.B conceived the research programme. C.K.,
L.S. and K.Y. designed the experiment; C.K. and L.S. conducted the research and
analysed the data; C.K. drafted the paper, which all authors critically revised and
approved

Correspondence:

Carmen Kohl
City University of London
Rhind Building
EC1V 0HB
London
carmen.kohl@city.ac.uk

Number of figures: 4

Number of Tables: 2

Number of Multimedia: 0

Number of words for Abstract: 243

Number of words for Significance Statement: 114

Number of words for Introduction: 707

Number of words for Discussion: 1996

Conflict of Interest: The authors declare no competing financial interests.

Funding Sources: This work was funded by a Leverhulme Trust Research Project
Grant (RPG-2014188).

37 **Abstract**

38 Evolutionary pressures suggest that choices should be optimised to maximise
39 rewards, by appropriately trading speed for accuracy. This speed-accuracy tradeoff
40 (SAT) is commonly explained by variation in just the baseline-to-boundary distance,
41 i.e. excursion, of accumulation-to-bound models of perceptual decision making.
42 However, neural evidence is not consistent with this explanation. A compelling
43 account of speeded choice should explain both overt behaviour and the full range of
44 associated brain signatures. Here, we reconcile seemingly contradictory behavioural
45 and neural findings. In two variants of the same experiment, we triangulated upon
46 the neural underpinnings of the SAT in the human brain using both EEG and TMS.
47 We found that distinct neural signals, namely the ERP centroparietal positivity (CPP)
48 and a smoothed motor-evoked potential (MEP) signal, which have both previously
49 been shown to relate to decision-related accumulation, revealed qualitatively similar
50 average neurodynamic profiles with only subtle differences between SAT conditions.
51 These signals were then modelled from behaviour by either incorporating traditional
52 boundary variation or utilising a forced excursion. These model variants are
53 mathematically equivalent, in terms of their behavioural predictions, hence providing
54 identical fits to correct and erroneous reaction time distributions. However, the
55 forced-excursion version instantiates SAT via a more global change in parameters
56 and implied neural activity, a process conceptually akin to, but mathematically
57 distinct from, urgency. This variant better captured both ERP and MEP neural
58 profiles, suggesting that the SAT may be implemented via neural gain modulation,
59 and reconciling standard modelling approaches with human neural data.

60

61 **Significance Statement**

62 Successful organisms need to make the right choice fast. To make such decisions,
63 we are regularly forced to trade speed for accuracy. This tradeoff has been
64 explained in behavioural models using a single free parameter reflecting response
65 caution. However, neural evidence suggests that more widespread changes are
66 associated with quick vs accurate decisions. Here, we suggest a model which
67 reconciles these seemingly contradictory findings. This 'forced-excursion' model is
68 mathematically equivalent to standard models of response caution but implies a
69 global modulation in activity akin to a change in neural gain or urgency. Re-
70 expressed in this way, the model is able to account for both behavioural and neural
71 data from two separate neural recording techniques.

72

73

74

75 Introduction

76 Every day we make countless decisions, each requiring an appropriate compromise
77 between speed and accuracy. This speed-accuracy tradeoff (SAT, Garrett, 1922;
78 Hick, 1952; Wickelgren, 1977) appears ubiquitous across experimental tasks and
79 species (Chittka et al., 2003; Heitz and Schall, 2012; Ivanoff et al., 2008). The
80 process of making decisions can be formally described using sequential sampling
81 models: Sensory evidence accumulates over time, until a decision boundary is
82 reached, triggering a response (Brown and Heathcote, 2008; Ratcliff, 1978). Such
83 models traditionally explain SAT-related changes in the reaction-time distributions of
84 both correct and erroneous responses by adjusting their boundary parameter. This
85 reduces the required accumulation excursion, leading to faster but more error-prone
86 decisions (Bogacz et al., 2006; Brown and Heathcote, 2008; Smith and Ratcliff,
87 2004; Usher and McClelland, 2001).

88
89 Signals displaying the accumulation predicted by these models have been identified
90 in electrophysiological data from non-human primates (Gold and Shadlen, 2000;
91 Shadlen and Newsome, 1996, 2001), and recently also in humans (Donner et al.,
92 2009; Hadar et al., 2016; O'Connell et al., 2012). However, when instructions or
93 payoffs change, neural accumulation profiles appear inconsistent with a changing
94 boundary, the traditional model-based explanation of the SAT (Hanks et al., 2014;
95 Heitz and Schall, 2012, 2013).

96
97 Hanks et al. (2014) proposed that the SAT is explained by an urgency signal in
98 monkeys. Similarly, a recent human neuroimaging study proposed that urgency may
99 arise from a global modulation of neural gain (Murphy et al., 2016). In fact, the

100 concept of an evidence-independent urgency signal, which increases over time to
101 inflate the accumulation process, has been a recurring theme in the recent SAT
102 literature (Cisek et al., 2009; Milosavljevic et al., 2010; Thura et al., 2012). This
103 urgency signal may increase faster under speed instructions, leading to faster, more
104 error-prone responses. However, alternative accounts, prioritising human
105 behavioural data, favour models which implement boundary differences (hereafter
106 referred to as “classic” models) as opposed to urgency signals (Hawkins et al., 2015;
107 see also Evans et al., 2017).

108

109 Here, we aimed to square these contrasting behavioural and neural findings. In
110 classic models, the use of a varying boundary to explain the SAT is in fact merely a
111 conceptually appealing convention. Since sequential sampling models are formally
112 non-identifiable (i.e. different parameter combinations can yield the same prediction),
113 one parameter must be chosen as a scaling parameter and fixed to an arbitrary
114 value (i.e. changing its value will lead to a change in the value of all parameters but
115 not in their relation to each other and therefore will not affect the model fits; Donkin
116 et al., 2009; Ratcliff and Rouder, 1998). This suggests that a variant of the classic
117 model could be used to transfer the effects of the SAT onto other model parameters,
118 while providing an equivalent fit to the data. We hypothesised that this mathematical
119 sleight of hand would reconcile the classic bound-variation explanation of the SAT
120 with neural findings.

121

122 We tested this hypothesis against data from two experiments. Experiment 1 used
123 transcranial magnetic stimulation (TMS) to track corticospinal excitability, a
124 downstream signal presumed to be under continuous influence from the decision

125 variable (Bestmann et al., 2008; Duque et al., 2010; Hadar et al., 2016; Klein-Flugge
126 and Bestmann, 2012). In Experiment 2, we recorded the event-related potential
127 (ERP) centroparietal positivity (CPP; Kelly and O'Connell, 2013; O'Connell et al.,
128 2012; Twomey et al., 2016), a large, late positivity recorded over parietal regions.
129 Importantly, this ERP has been suggested to reflect decision-related accumulation
130 directly, independently of associated motor responses. These ERP and MEP signals
131 therefore represent fundamentally different neural generators, which have both been
132 shown to reflect decision-making processes. We believe that this methodological
133 triangulation permits a more robust interpretation that spans the sensorimotor
134 pipeline.

135

136 In both experiments, participants made decisions with two difficulty levels under SAT
137 instructions. Difficulty influences the rate of evidence accumulation (Donkin et al.,
138 2011; Ratcliff and McKoon, 2008), and was introduced here to confirm that our
139 signals represented plausible correlates of the decision variable. We then
140 constructed accumulation profiles predicted when the SAT is modelled through
141 boundary variations, and by our alternative forced-excursion approach. By
142 comparing these neurodynamic predictions to data, we demonstrate that classic
143 models re-expressed to have a fixed excursion provide compelling approximations to
144 both brain and behavioural measures in humans.

145

146 **Materials & Methods**

147 **Participants**

148 For the TMS experiment, an opportunity sample of 22 participants (13 female),
149 primarily students and staff at City, University of London were recruited. According to
150 criteria established prior to the experiment, participants were excluded if they were
151 unable to reach a calibrated coherence level of less than 90% for either of the
152 difficulty conditions (see *Difficulty Calibration*). The remaining 18 participants (11
153 female, mean age of 29.82, $SD = 8.38$) took part in three sessions, each lasting
154 between 2 and 2.5 hours and involving the same conditions (speed/accuracy
155 easy/hard, see below). For the EEG experiment, we recruited 26 participants (17
156 females). Of these, 23 (15 females), with a mean age of 29.39 ($SD = 7.47$), pre-
157 tested sufficiently well to proceed to the main experiment, and thus participated in a
158 single 2-hour session. All participants were paid £8 per hour and an additional
159 reward for task performance (up to £4 per session). The experiments were approved
160 by the City, University of London Psychology Department Ethics Committee.

161

162 **Stimuli and Procedure**

163 < Insert Figure 1 around here >

164 **Stimuli and Experimental setup**

165 In the random dot motion task (Figure 1 a), participants saw an array of moving
166 dots, a proportion of which moved coherently in one direction (equiprobably up or

down) while the rest moved in random directions (selected for each dot on each frame). Trial difficulty was manipulated by varying the proportion of dots moving coherently. The task was displayed on a cathode ray tube (CRT) screen (size: 41 cm x 30 cm), operating at a refresh rate of 85 Hz and a resolution of 1240 x 786 pixels. Participants sat at a distance of 100 cm from the screen. In each trial, 300 white dots, each 0.04 x 0.04 degrees visual angle (dva) in size, were displayed within a 5 dva aperture on a black background. A fixation cross (size: 0.33 x 0.33 dva) was located centrally. All dots moved at a speed of 3.3 dva per second. The position of all dots was randomised every five frames. The experiment was coded in Matlab (The Mathworks, Natick, U.S.A.), using the Psychophysics Toolbox extension (Brainard, 1997; Kleiner et al., 2007; Pelli, 1997) and run on a PC.

Initially, participants saw a fixation cross for 500 ms (plus a jitter of up to 1000 ms, drawn from a uniform distribution). Then, 100% of the dots moved randomly for 1000 ms (plus a jitter of up to 1500 ms, drawn from a truncated gamma distribution with shape parameter 1 and scaling parameter 150). This was followed by the onset of coherent motion, either upwards or downwards, for up to 2000 ms, or until response. Feedback was provided after each trial (see *SAT Instructions*). Two equiprobable coherence levels generated 'easy' (high coherence) and 'hard' (low coherence) trials, which were randomly intermixed. The 'speed' and 'accuracy' conditions were blocked. The order of these SAT blocks was counterbalanced across participants.

Each participant completed a minimum of 100 practice trials, followed by 200 calibration trials (see *Difficulty Calibration*). In each experimental TMS (EEG) session, a total of 432 (800) planned trials were completed, and self-timed breaks

192 were provided after every 50 (100) trials. In TMS sessions, to ensure the required
 193 frequency of pulses ($< .2$ Hz), TMS-free trials were added when necessary (see *TMS*
 194 *and EMG Processing*), leading to an average of ~500 trials per session.

195

196 **Responses**

197 Participants in the TMS experiment held two digital response buttons interfaced via a
 198 16 bit A/D card (National Instruments X-series PCIe-6323, sample rate 100,000 Hz)
 199 in their right hand. One button was placed between the thumb and index finger and
 200 required a 'pinch' response, contracting the first dorsal interosseous (FDI) muscle.
 201 The second button was placed on a plastic cylinder in the palm of the hand and
 202 required a 'grasp' response, contracting the abductor digiti minimi (ADM) muscle
 203 (Figure 1 b). The pinch and grasp buttons indicated 'up' and 'down' responses
 204 respectively. In the EEG experiment, participants held one button between the thumb
 205 and index finger of each hand, with right and left-hand button presses indicating
 206 upward and downward motion respectively.

207

208 **Difficulty Calibration**

209 Once participants felt comfortable with the task, they completed a total of
 210 200 staircase trials to calibrate the level of difficulty appropriate for the 'easy' and
 211 'hard' conditions. A QUEST procedure (Watson and Pelli, 1983) estimated the
 212 coherence levels at which each participant responded correctly in 75% and 95% of
 213 trials, used for the 'hard' and 'easy' conditions respectively. The stimulus
 214 presentation time was reduced from 2000 ms to 1300 ms, and no feedback was

215 provided during QUEST trials. If a participant's performance led to estimated hard
216 coherence levels of more than 90%, the participant was excluded from the
217 experiment. This procedure resulted in a mean coherence of 23.81% in the hard
218 condition and 65.41% in easy trials in the TMS experiment, and 30.63% for hard,
219 and 67.67% for easy trials in the EEG experiment.

220

221 **SAT Instructions**

222 After the difficulty calibration, the main experiment began, in which, participants
223 were instructed to react either as fast or accurately as possible in different blocks.
224 Additionally, feedback was provided after each trial to either reward participants (by
225 display of the word 'Correct' and a small monetary reward, adding up to a maximum
226 of £4 per participant) for fast and correct/correct responses in 'speed'/'accuracy'
227 trials respectively, or provide negative feedback (with the words 'TOO SLOW' or
228 'INCORRECT' in green letters on a red screen) when the instructions were not
229 followed. The inter-trial interval was increased by 1000 ms after each trial with
230 negative feedback. Neutral feedback (no monetary reward, but a neutral screen with
231 the words 'incorrect' or 'too slow') was shown when participants responded fast but
232 incorrectly in the 'speed' condition or accurately but very slowly in the 'accuracy'
233 condition. Whether a response was too slow or not was determined by a variable
234 deadline which was initially set to 600 ms for the 'speed' and 1000 ms for the
235 'accuracy' condition. To optimise performance, the deadlines varied between 450
236 and 750 ms ('speed') and between 700 and 1300 ms ('accuracy') and were adjusted
237 using separate QUEST procedures, targeting accuracy levels of 75% for 'speed',

238 and 90% for 'accuracy' conditions. Feedback was also provided when participants
239 responded before the onset of the coherent motion ('too fast').

240

241

242 **TMS and EMG Processing**

243 In the TMS experiment, participants' muscle activity was recorded using surface
244 electromyography (EMG), sampled at 1000 Hz via a 13 bit A/D Biometrics Datalink
245 system (version 7.5, Biometrics Ltd., Ladysmith, VA, U.S.A., 2008). We placed 22
246 mm x 28 mm surface Ag/AgCL electrodes on the skin above the FDI and the ADM of
247 the right hand, as they contribute to the 'pinch' and 'grasp' responses respectively.
248 Reference electrodes were placed at distances of approximately 2 cm to each active
249 electrode. Participants were instructed to relax their hand muscles in between
250 responses, and the EMG signals were passed to two speakers to provide auditory
251 feedback about any unwanted muscle activation.

252

253 During the experiment, single-pulse TMS was applied using a MagstimRapid²
254 biphasic stimulator (Magstim Co. Ltd., Whitland, UK). A figure-of-eight coil was
255 positioned over the optimal spot on the scalp over the left primary motor cortex to
256 elicit MEPs in both the ADM and FDI. The exact location was adjusted for each
257 participant and the stimulation intensity was set at approximately 110% of the resting
258 motor threshold, in order to evoke potentials of around 1 mV in both muscles. The
259 resting motor threshold was defined as the minimal intensity necessary to elicit an
260 MEP with a peak-to-peak amplitude of ~50 μ V in 50% of stimulations in both the FDI

261 and the ADM, and was, on average, 59.28% ($SD = 7.76$) of maximum stimulator
262 output.

263

264 TMS pulses were planned in 66% of trials, but cancelled if a response was detected
265 before stimulation. To ensure a good distribution of TMS pulses over the course of
266 the reaction time, TMS trials were divided into four equally sized, equiprobable time
267 bins (between 5 ms and 500 ms relative to the onset of the coherent motion in the
268 'speed' condition, and between 5 ms and 600 ms in the 'accuracy' condition). Within
269 a given bin, the exact stimulation time was drawn uniform randomly. Since the
270 experiment followed a single-pulse TMS protocol, pulses were required to occur at a
271 maximal frequency of 0.2 Hz. If, by chance, a planned pulse followed a previous one
272 after less than 5000 ms, the task was adjusted in several ways. If the timespan
273 between the previous and the planned pulse was less than 5000 ms but more than
274 4000 ms, the inter-trial interval was increased in order to decrease the pulse
275 frequency to < 0.2 Hz. For scheduled intervals of less than 4000 ms, the planned trial
276 was replaced with the next planned stimulation-free trial. If no stimulation-free trial
277 remained, random stimulation-free trials were generated in order to increase the
278 interval between TMS pulses, resulting in an average of 68.67 ($SD = 15.79$)
279 additional trials per session.

280

281 **EMG pre-processing**

282 To eliminate potential differences in the time required to execute 'pinch' and 'grasp'
283 responses, we recorded the onset of EMG as a measure of reaction time (EMG RT).
284 EMG data from both channels were aligned to the onset of the coherent motion

285 (stimulus onset) and visually inspected to select the onset of response-related EMG
 286 bursts. Visual inspection provided no information about the experimental condition of
 287 a given trial.

288

289 In TMS trials, MEP amplitudes in both channels (FDI and ADM) of the right hand
 290 were defined as the difference between the minimal and maximal EMG values in a
 291 time window of 10 to 40 ms relative to stimulation time. An algorithm detected EMG
 292 activity prior to the stimulation, discarding any trials in which there was activity
 293 greater than 50 μ V peak to peak in a period of 200 ms preceding the stimulation.
 294 These trials, as well as trials in which there was partial activation in more than one
 295 channel, or trials in which a clear EMG onset could not be detected, were excluded
 296 from further analysis (23.39% of trials). Additionally, trials with very fast (< 100 ms) or
 297 very slow (> 1800 ms) response onsets (5.12% of trials), trials in which no MEP was
 298 visible or in which the MEP amplitude could not be accurately detected due to
 299 amplifier saturation (1.05%), and trials in which the response preceded the planned
 300 TMS pulse (6.09%) were excluded. In total, 35.65% of all trials were discarded, with
 301 a total of 17,067 trials remaining, including 6535 usable TMS trials (42.85% of all
 302 planned TMS trials).

303

304 **MEP processing**

305 To yield sufficient data to accurately estimate corticospinal excitability in a time-
 306 continuous manner, correct-trial MEPs from all participants were combined. Before
 307 pooling, MEP amplitudes were z-transformed separately for each muscle, session
 308 and participant, while TMS latencies were normalised by median RT of TMS-free

309 trials in the corresponding session. Z-scored MEPs were then sorted as a function of
 310 stimulation latency (Figure 1 c, e, f) and smoothed using a Gaussian kernel to
 311 recover a continuous time-varying MEP average in steps of 1% median RT:

312

$$313 \quad (1) \quad \hat{Y}(t) = \frac{\sum_{i=1}^N e^{-\frac{(t-t_i)^2}{2\sigma^2}} Y_i}{\sum_{i=1}^N e^{-\frac{(t-t_i)^2}{2\sigma^2}}}$$

314

315 Where the N contributing MEPs each have amplitude Y_i and occur at normalised
 316 time t_i . The width of the Gaussian kernel defined by the full width half maximum was
 317 set at 5% of median RT (i.e., around 20ms), previously suggested as an appropriate
 318 compromise between temporal resolution and signal-to-noise ratio (Hadar et al.,
 319 2016). This MEP signal was computed for both stimulus and response-locked MEP
 320 latencies, and from the responding muscle, the non-responding muscle and the MEP
 321 amplitude difference between them. Finally, 95% confidence intervals were
 322 estimated around each signal using a bias-corrected and accelerated bootstrap
 323 (BCa) confidence interval, based on 1999 iterations. Since analyses were restricted
 324 to correct trials, MEPs recorded from the responding muscle always reflected
 325 activation of the correct response, while MEPs from the non-responding muscle
 326 reflected the incorrect response. We focused particularly on the MEP average signal
 327 based on the amplitude difference between responding and non-responding MEPs,
 328 as this eliminates variations due to non-specific influences, such as inhibitory
 329 processes during action preparation, which would result in MEP suppression in both
 330 responding and non-responding muscles (for a review see Duque et al., 2017).

331

332

EEG Recording and Processing

Continuous EEG was recorded using 64 active electrodes, placed equidistantly on the scalp (EasyCap, M10 Montage) and referenced to the right mastoid (BrainAmp amplifier; BrainProducts; sampling rate: 1000 Hz). The data were pre-processed and analysed using custom scripts in Matlab (Mathworks, Natick, USA), drawing on functions from the EEGLAB toolbox (Delorme and Makeig, 2004).

EEG data were re-referenced to the average reference and digitally bandpass filtered (0.1 to 45 Hz). Data were visually inspected to remove large muscle artefacts before applying ICA to remove eye blink components. Any remaining artefacts were removed manually during a second visual inspection. Afterwards, spherical spline interpolation was used to reconstruct noisy channels, which were identified and rejected during the first visual inspection. In line with the procedures used in previous CPP studies (Kelly and O'Connell, 2013; O'Connell et al., 2012), the data were converted to current source density (CSD) estimates using the CSD toolbox (Kayser and Tenke, 2006).

Experimental Design and Statistical Analysis

Behavioural Data Analysis

We explored the within-subjects factors Instruction and Difficulty with the levels speed/accuracy and easy/hard respectively. To test their effects on RT, we used a 2x2 repeated-measures ANOVA. Because accuracy data violate the assumptions of ANOVA, statistical inferences about errors were made using a generalised linear

356 mixed-effects model with a logistic link function and binomial data model (applied
 357 using the 'fitglme' function in Matlab). Parameter estimates were based on a
 358 maximum-likelihood method using Laplace approximation and the 'maximal' random
 359 effects structure (Barr et al., 2014), i.e. both Instruction and Difficulty, and the
 360 Instruction*Difficulty interaction were entered as fixed effects, and both
 361 manipulations, and their interaction within each participant (and session in the TMS
 362 experiment) were included as random effects.

363

364 **MEP Analysis**

365 Two analyses were conducted on the MEP difference signal to confirm that MEP
 366 modulations across time reflected decision-related accumulation processes. We
 367 compared the stimulus-locked build-up rate, expected to be steeper in easy than
 368 hard trials, and the response-locked signal amplitude, which should not vary across
 369 difficulty levels at the time of decision. Comparisons were also made across speed
 370 instructions, although no clear predictions could be made regarding how evidence
 371 accumulation should vary in this case. MEP data were permuted across easy and
 372 hard (or across speed and accuracy) trials 1999 times. Mean MEP signals (and 90%
 373 BCa confidence intervals; see below) were then computed for each iteration. The
 374 build-up rate was then estimated from both the original and the resampled data as
 375 the slope of a straight line fitted to the stimulus-locked signal in a time window
 376 ranging from half median up to median RT (corresponding to around 200 to 400 ms
 377 after stimulus onset). Slope differences between difficulty levels or instructions were
 378 considered significant if smaller (or larger) than the lower (or upper) 2.5% of the
 379 corresponding slope-difference null distribution obtained from resampled signals.

380

381 To test response-locked amplitude differences while controlling for multiple
382 comparisons, a cluster statistic was calculated (c.f. Blair and Karniski, 1993; Groppe
383 et al., 2011; Nichols and Holmes, 2001). Potential regions of difference between
384 conditions were based on contiguous time periods with no overlap between 90%
385 bootstrap BCa confidence intervals (the arbitrary “cluster threshold”). A cluster sum
386 was calculated within each such putative cluster, and was considered significant
387 when this sum of the point-by-point differences fell outside the central 95% of the
388 corresponding distribution of the biggest cluster sum obtained from resampled
389 signals. Amplitude differences were assessed on both stimulus and response-locked
390 signals.

391

392 **ERP Analysis**

393 For the ERP analysis, we extracted both stimulus (-200 to 2000 ms, relative to
394 coherent motion onset) and response aligned (-1000 to 100 ms, relative to the button
395 press) epochs. All epochs were baseline corrected to the average over a 200 ms
396 period preceding motion onset. The appropriate electrode to generate the CPP
397 waveform was chosen individually, by visually inspecting each participant’s averaged
398 ERP topography to identify the centroparietal region of maximum amplitude (chosen
399 electrodes: 1, 5, or 14, roughly equivalent to electrodes Cz, CPz, Pz in the 10-20
400 system). The activity recorded on the selected electrode was averaged for each
401 condition (collapsed over ‘up’ and ‘down’ trials) and for stimulus and response-locked
402 signals separately. In line with Kelly and O’Connell (2013), we measured the slope of
403 the CPP for each participant, by fitting a straight line to the waveform from 200 to

350 ms in the stimulus-locked data. Additionally, we measured the peak amplitude of the response-locked ERP by averaging over the amplitude of the waveform from -50 to 50 ms relative to the response. Differences across conditions were assessed with a 2x2 repeated-measures ANOVA.

408

409 **Modelling**

410 **Free-excursion race model**

411 According to a standard free-excursion race model (Bogacz et al., 2006; Laberge, 1962; Vickers, 1970) evidence supporting the correct and the incorrect response is integrated independently in two accumulators. The amount accumulated at each time step (dx) is given by:

415

$$\begin{aligned} 416 \quad & dx_{\text{correct}} \propto v_{\text{correct}} + N(0, \sigma^2) \\ 417 \quad (2) \quad & dx_{\text{incorrect}} \propto v_{\text{incorrect}} + N(0, \sigma^2) \end{aligned}$$

418

419 Where x_{correct} and $x_{\text{incorrect}}$ are the quantities accumulated, and v_{correct} and $v_{\text{incorrect}}$ the input evidence (i.e. accumulation rate, see below) in favour of the correct and the incorrect responses. Noise, N , drawn from a normal distribution of mean 0 and standard deviation σ , is also integrated at each iteration. To avoid negative values, evidence accumulated at each time step is updated as:

424

$$\begin{aligned} 425 \quad & x_{\text{correct}}(t+1) = \max(0, x_{\text{correct}}(t) + dx_{\text{correct}}) \\ 426 \quad (3) \quad & x_{\text{incorrect}}(t+1) = \max(0, x_{\text{incorrect}}(t) + dx_{\text{incorrect}}) \end{aligned}$$

427

428 Correct and incorrect accumulator starting points are drawn in each trial from a
 429 uniform distribution ranging between 0 and S_z . As soon as one of the accumulators
 430 reaches the response boundary A , the corresponding response is selected. The
 431 response time is then modelled as the time required to reach the boundary, plus
 432 non-decision time, during which sensory and motor processes occur, drawn from a
 433 uniform distribution centred on T_{er} and of width S_{Ter} . In a standard race model for a
 434 binary decision, this leads to a total of seven parameters (A , S_z , $v_{correct}$, $v_{incorrect}$, T_{er} ,
 435 S_{Ter} , σ^2). One parameter is chosen as a scaling parameter and fixed to an arbitrary
 436 value, resulting in a total of six free parameters.

437

438 To apply this model to the data in this experiment, we added accumulation rate
 439 parameters to account for the different difficulty conditions ($v_{easy_correct}$, $v_{easy_incorrect}$,
 440 $v_{hard_correct}$, $v_{hard_incorrect}$). This implementation of difficulty is well-established and has
 441 been validated using both behavioural and neural data (Mulder et al., 2014; Ratcliff
 442 and McKoon, 2008; Ratcliff and Rouder, 1998; Roitman and Shadlen, 2002; Twomey
 443 et al., 2015). In order to explain differences due to SAT instructions, we added a
 444 second boundary parameter. The boundary for ‘accuracy’ trials $A_{accuracy}$ acted as a
 445 scaling parameter and was fixed to 1, while the boundary for the ‘speed’ condition,
 446 A_{speed} , was free to vary. We tested three different models: one in which all remaining
 447 parameters were fixed across conditions (Model 1), one in which the starting point
 448 parameter S_z was free to vary across SAT conditions (Model 2), and one in which the
 449 non-decision time parameter T_{er} was free to vary across SAT conditions (Model 3;
 450 see Table 1).

451 Modelled RTs were simulated based on Equations 2 and 3 (10,000 simulated trials
 452 with a 1% median RT time step, around 4ms, for TMS and a 10ms time step for
 453 EEG) and compared to pooled RT data using Quantile Maximum Probability
 454 Estimation (Heathcote et al., 2002). Specifically, we estimated empirical RT quantiles
 455 (at 0.1, 0.3, 0.5, 0.7 and 0.9), for both correct and erroneous responses, and
 456 compared counts of simulated RTs in the resulting bins against the predicted
 457 multinomial distribution. Parameter values were adjusted using a differential
 458 evolution algorithm implemented in Matlab (Price et al., 2005). The goodness-of-fit of
 459 the different models was assessed by computing the Akaike information criterion
 460 (AIC, Akaike, 1977).

461

462 **Forced-excursion Race model variant**

463 To test the hypothesis that the SAT is not implemented through decision bound
 464 variation *per se*, but rather by more widespread changes of neural activity, we
 465 constructed a forced-excursion model variant in which decision boundaries are fixed
 466 and the effects of the SAT are transferred onto all other parameters. All parameters
 467 of the free-excursion race model estimated in the speed condition were divided by
 468 the speed boundary A_{speed} (apart from T_{er} and S_{Ter}). This forced-excursion version of
 469 the model is mathematically equivalent to the original one as, given the scaling
 470 property of sequential sampling models, multiplying all models parameters (except
 471 T_{er} and S_{Ter}) by the same amount does not affect model predictions (Donkin, Brown,
 472 et al., 2009). A simple 'rescaling' of speed parameters hence results in a new set of
 473 parameters in which the speed and accuracy response boundaries are equal, and
 474 the SAT modulation is transferred onto the other decision-related parameters.

475

476 **Model predictions**

477 *TMS experiment:* In each session, EMG RTs were normalized by median EMG RT,
478 and trials were pooled across sessions and participants. On average, we obtained
479 2,651 trials per condition, used to determine best-fitting parameters at the group
480 level. We then generated predictions according to the free and forced-excursion race
481 model variants by simulating evidence accumulation. To allow for a direct
482 comparison, model predictions were constructed identically to the accumulation
483 signals derived from our experimental data, i.e., as MEP difference average signals.

484

485 For both models, and each condition, 20,000 single-trial accumulation paths were
486 computed based on Equations 2 and 3 (in 0.5% median EMG RT time steps). Each
487 modelled MEP amplitude was determined by the value of one of the single-trial
488 simulated accumulation signals reached at a (simulated) TMS latency, based on
489 stimulation times applied during the experiment (see Figure 1 d-f). The difference
490 between correct and incorrect values was used to model the MEP difference signal.
491 As in experimental data, trials were discarded when simulated RT was shorter than
492 TMS latency (i.e., the response would have been given before the TMS pulse). The
493 duration of sensory and motor processes, which are represented by a single T_{er}
494 parameter, have to be allocated to pre and post-accumulation processes in order to
495 generate predictions. Since we modelled accumulation observed in or around M1,
496 we assumed that post-accumulation stages would only relate to response execution,
497 which could reasonably be ignored, as reaction times were defined up to EMG onset.

498 Therefore, the whole of T_{er} was allocated to pre-accumulation processes, and
 499 accumulation started after a delay of $T_{er} \pm S_{Ter}$.

500

501 From simulated MEPs, predicted continuous MEP signals were then computed by
 502 applying the same smoothing method applied to the MEP data. Finally, accumulation
 503 signals based on predicted MEPs were compared to the empirical MEP signal using
 504 a mean squared error metric, after a scaling procedure was applied to match
 505 modelled and experimental signal amplitudes. Modelled signals were vertically
 506 normalized by the value minimizing the mean squared error, estimated using the
 507 previously described differential evolution algorithm. Note that even though this
 508 normalization could differ between the free and forced-excursion models, the same
 509 value was applied within each model to all conditions, and to stimulus and response-
 510 locked signals.

511

512 Finally, two complementary statistical analyses compared the mean squared errors
 513 obtained for the free and forced-excursion model variants, to determine which
 514 predictions displayed greater similarities to the neural signal. First, goodness-of-fit of
 515 the model predictions was computed based on AIC values, using the formula $AIC =$
 516 $n \cdot \log(MSE) + 2K$ (Burnham and Anderson, 2004), where n is the number of
 517 observations, MSE the mean squared error, and K the number of free parameters
 518 ($K=1$ in this case, as only amplitude was allowed to vary freely to fit recorded MEP
 519 signals). AIC was then used to compute Akaike *model weights*, which can be seen
 520 as the weight of evidence in favour of each model.

521

522 The second analysis applied a bootstrap procedure estimating the distribution of
 523 differences of mean squared error between the free and forced-excursion models, in
 524 order to determine the bias-corrected¹ 95% confidence interval around the observed
 525 difference. To estimate the distribution, EMG RT data were resampled 1999 times
 526 with replacement within each condition. The best-fitting parameters for the original
 527 and each resampled set of EMG RT data were then estimated by a simplex
 528 algorithm implemented in Matlab (Lagarias et al., 1998), using the original
 529 parameters as starting values². As for the original analysis, forced-excursion
 530 parameters were obtained by normalising the free-excursion parameters by the
 531 response boundary value obtained in the speed condition, and MEP signal
 532 predictions for free and forced-excursion models were computed. Mean squared
 533 errors were then calculated between these bootstrapped signal predictions and a set
 534 of equivalently resampled MEP signals, again after applying a scaling procedure
 535 matching signals amplitudes (via a differential evolution algorithm, Price et al., 2005).
 536 The 95% bias-corrected confidence interval was estimated based on the bootstrap
 537 distribution of mean squared error differences between the free and forced-excursion
 538 models.

539
 540 *EEG experiment:* RTs were pooled across participants to fit the models at a group
 541 level. As EEG signals integrate spatially disparate underlying neuronal activity, we
 542 reasoned that the CPP would likely represent the sum of evidence accumulators
 543 across time. The corresponding accumulation signals predicted by the models
 544 should therefore be obtained by adding up the correct and incorrect accumulators'

¹ Bias-correction was used rather than bias-correction and acceleration (BCa) to make the time of computation manageable.

² The Simplex algorithm was preferred to the differential evolution algorithm in this case to reduce the time of computation.

activities. For both models and each speed and coherence level condition, 10,000 single-trial accumulation paths were computed based on Equations 2 and 3. To account for sensory processes, accumulation started after a sensory delay. Once a decision was made, we assumed that evidence accumulation continued until the response was executed (and the stimulus was turned off). Accumulation therefore continued after the boundary was reached for the duration of any motor processes (Resulaj et al., 2009; Twomey et al., 2015). The compound duration of sensory and motor processes were given by the model non-decision time T_{er} , which we divided into T_e and T_r , modelling sensory and motor processes respectively. As detailed below, this division was optimized for each model. To match with EEG processing, the sum-of-accumulations signal was baseline corrected by subtracting the first data point value from each trial. Finally, to compare the prediction to the CPP, we averaged accumulation signals in each condition, either time-locked on stimulus onset (i.e., time 0), or on response time (the time of the corresponding simulated RT). Since we can only speculate on how the accumulator behaves once the response is executed, trials were removed from averaging once the simulated response time had been reached (and the same procedure was used for the averaging of empirical EEG data).

The similarity between the CPP and the predicted decision variable of each model was quantified by computing the mean squared error between mean signals. To provide optimal CPP predictions, the amplitude of each summed signal was scaled to match the CPP amplitude, and the division of non-decision time T_{er} into encoding time T_e and response time T_r was determined. The optimal scaling factor and T_{er}

569 division were obtained for each model signal using differential evolution (Price et al.,
 570 2005), minimising the mean squared error.
 571
 572 Finally, as in the TMS experiment, a bootstrap analysis (bootstrapping both RT and
 573 EEG data) determined whether the mean squared error calculated for the free- and
 574 the forced-excursion models had a 95% confidence interval excluding zero, i.e.
 575 whether they differed significantly. In this experiment, no AIC-based comparison was
 576 attempted because EEG data points have complex temporal dependencies (i.e.
 577 autocorrelation) that make it difficult to establish the likelihood with which a model
 578 predicts these neurodynamic data.
 579

580 Results

581 Behavioural Results

582 Trials remaining after pre-processing were collapsed over 'up' and 'down' trials
 583 (Figure 2). Both experiments revealed the same behavioural effects. As expected,
 584 RTs were faster under speed than accuracy instructions (TMS: $F(1,17) = 26.90$, $p <$
 585 $.001$, $\eta_p^2 = .61$; EEG: $F(1,22) = 36.47$, $p < .001$, $\eta_p^2 = 0.62$), as well as in easy
 586 compared to hard trials (TMS: $F(1,17) = 62.14$, $p < .001$, $\eta_p^2 = .79$; EEG: $F(1,22) =$
 587 120.12 , $p < .001$, $\eta_p^2 = 0.85$). Additionally, Instruction and Difficulty interacted (TMS:
 588 $F(1,17) = 10.80$, $p = .004$, $\eta_p^2 = .79$; EEG: $F(1, 22) = 36.47$, $p < .001$, $\eta_p^2 = .62$).
 589 Follow-up t-tests revealed that the effect of difficulty was larger in the accuracy
 590 condition ($p < .001$) than in the speed condition ($p < .001$). All reported effects in the

591 TMS experiment are based on EMG RT (time of EMG onset), but results based on
 592 response-button RT were not qualitatively different.

593

594 For error data, a generalised linear mixed-effects model revealed higher accuracy
 595 scores under accuracy compared to speed instruction (TMS: $t(208) = 4.81$, $p < .001$;
 596 EEG: $t(88) = 7.76$, $p < .001$), as well as in easy trials compared to hard trials (TMS:
 597 $t(208) = 4.57$, $p < .001$; EEG: $t(88) = 4.68$, $p < .001$). The Instruction*Difficulty
 598 interaction was not significant ($p > .05$).

599

600 < Insert Figure 2 around here >

601 **Neural Results**

602 **MEP-average signals**

603 MEP amplitudes from correct trials were collated and smoothed to form three
 604 categories of MEP-average signal: Responding, non-responding, and the difference
 605 between them. Responding and non-responding MEP-average signals obtained for
 606 each condition are presented in Figure 3 a. The responding MEP-average signal
 607 (associated with the correct response) builds up gradually during the reaction time
 608 period, while the non-responding signal (associated with the incorrect response)
 609 remains fairly flat. However, our main focus was the difference in MEP amplitudes
 610 between responding and non-responding muscles (Figure 3 c). Statistical analyses
 611 confirmed that this MEP signal displays characteristics consistent with the
 612 hypothesis that M1 excitability reflects an accumulation process. We found that the
 613 stimulus-locked signal built up faster in easy than hard trials (for both speed, $p =$

614 .049, and accuracy, $p < .001$ instructions), and that the response-locked signal
 615 amplitude reached similar levels just before the response regardless of trial difficulty,
 616 with cluster permutation tests showing no significant divergence between conditions
 617 ($p = 1$). Differences were however observed in stimulus-locked averages, with higher
 618 amplitudes evident in easy compared to hard trials from 75% median EMG RT (~294
 619 ms) in the speed condition ($p = .005$) and from 81% (~318 ms) under accuracy
 620 instructions ($p < .001$). The latter results demonstrate that we had sufficient power to
 621 detect MEP amplitude differences. Collectively, our results show that the MEP-
 622 average difference signal is a viable neural correlate of the decision variable.
 623 However, no difference was observed between speed and accuracy instructions, on
 624 either the slope or amplitude of MEP accumulation (all $p > .1$).

625

626 ERP Results

627 The CPP is displayed in Figure 3 b. Like the MEP-average difference signal, it builds
 628 over the course of the decision, at a rate reflecting the difficulty of the decision. For
 629 build-up rate, there was a significant main effect of Difficulty ($F(1,22) = 14.70$, $p =$
 630 $.001$, $\eta_p^2 = .40$), with higher slopes in easy compared to hard trials. There was no
 631 main effect for Instruction, and no interaction, in either of the time alignments ($p >$
 632 $.26$).

633

634 There was also a main effect of Difficulty on the peak amplitude of the response-
 635 locked CPP, $F(1,22) = 8.53$, $p = .008$, $\eta_p^2 = .28$, with higher amplitudes in the easy
 636 compared to the hard conditions. However, again we found no main effect for SAT
 637 Instruction and no interaction ($p > .22$).

638

639 Summarising the neural data, neurodynamic signals derived from two very different
 640 imaging methods converged to yield the same outcome: Clear effects of adjusting
 641 task difficulty, particularly on the rate of accumulation, but no statistically reliable
 642 effects of speed/accuracy instruction, despite the fact that these two manipulations
 643 had similar magnitudes of behavioural effect (mean RT effect sizes, i.e. η_p^2 , of 0.62
 644 for SAT instruction vs 0.82 for difficulty).

645

646

< Insert Figure 3 around here >

647

648

Model selection

649

650 In both experiments, we fitted several models to RT data and used AIC to select the
 651 best candidate with which to go on and make neural predictions. The winning race
 652 model (Model 2; see Table 1) varied both response boundary and starting-point
 653 between different SAT instructions (and also varied drift rates with changes in
 654 difficulty). As anticipated, the best-supported model's best-fitting parameters (shown
 655 under "free-excursion" in Table 2) show that the response boundary decreased
 656 under speed instruction, and that accumulation rates were higher for easy than hard
 657 trials. Additionally, starting-point variability was larger under speed instructions.
 658 Since the starting-point distribution ranges from 0 to the starting-point parameter S_z ,
 659 larger starting-point variability also implies a larger mean starting-point, further
 660 decreasing the distance between baseline and boundary. The quality of the fit was
 661 good (see Figure 4).

661

662 < Insert Figure 4 around here >

663 < Insert Table 1 around here >

664 < Insert Table 2 around here >

665

666 Importantly, we also re-expressed this model under a forced-excursion constraint. In
667 this forced-excursion version, parameter normalisation forced the speed response
668 boundary to be the same as the accuracy boundary, with the SAT being transferred
669 onto accumulation rate and variability parameters. Note that the forced-excursion
670 version of this model is mathematically equivalent to the standard one, with identical
671 predicted RTs and error rates.

672

673 Stimulus and response-locked accumulation signals for each experiment and each
674 condition predicted by the free and forced-excursion variants of the best-supported
675 model are shown in the lower panels of Figure 3. Broadly the same patterns were
676 predicted in both experiments. The main difference between free and forced-
677 excursion predictions is the level of accumulation reached at the time of the decision.
678 This is evident in the amplitude of response-locked signals attained just before
679 response selection, which is predicted to be higher under accuracy than speed
680 instructions for the free-excursion model, but similar in the forced-excursion model
681 (Figure 3 panels d-h). Note that, while this pattern is more pronounced in the forced-
682 excursion predictions associated with the MEP signal (Figure 3 e) than the EEG
683 signals (Figure 3 h), the reduced amplitude difference between speed and accuracy
684 profiles prior to the response is evident in both experiments, and importantly, both
685 forced-excursion model predictions capture the patterns seen in the corresponding
686 neural data (Figure 3 c, f). In the stimulus-locked predictions, easy trials display a

687 steeper build-up than hard trials, yet, interestingly, even though accumulation rates
688 in the forced-excursion model were higher under speed than accuracy instructions
689 (see Table 2), the predicted signal was not correspondingly steeper in this case (see
690 Figure 3 panels e, h). For MEPs, this may be partly explained by the fact that both
691 correct and incorrect accumulation rates increased, such that the slope of the
692 (motoric, thus difference-based) accumulation signal remained unaffected. However,
693 the similar pattern observed in CPP predictions (which were modelled as a sum of
694 accumulators, because this signal occurs relatively early and is not response-
695 specific) indicates that the ~20% change in modelled accumulation rate was
696 insufficient to generate a substantial increase in predicted slope when combined with
697 the associated changes in noise parameters.

698
699 Summarising these observations, the signals predicted by the forced-excursion
700 version of the best-supported model appear to better reproduce the pattern of the
701 recorded CPP and MEP signals than do those predicted by the free-excursion
702 version. Specifically, the accumulation slope is steeper in easy than hard trials, but
703 not different between speed and accuracy conditions, and a similar signal amplitude
704 is attained before response for both coherence levels, and, crucially, under both SAT
705 instructions.

706
707 Statistical analyses confirmed these observations. Akaike weights in the TMS
708 experiment indicated that neurodynamic predictions from the forced-excursion model
709 variant were better matched to the MEP signals than were free-excursion predictions
710 (forced-excursion: 0.994, free-excursion: 0.006). Additionally, bootstrap analysis
711 showed that the mean squared error between predicted MEP signals and recorded

MEP values was significantly lower for the fixed than the free-excursion model ($p = .018$, 95% bias-corrected confidence interval on difference: $[0.005; 0.056]^3$). The same bootstrap analysis revealed similar results in the EEG experiment, where the forced-excursion model predicted profiles more similar to the CPP than the free-excursion model ($p = .026$, 95% bias-corrected confidence interval on this difference: $[1.55; 21.32]^4$).

³ Although a significant difference was observed using a BCa confidence interval, this was not the case when a simpler percentile interval was used. This result should hence be interpreted cautiously (but is bolstered by our subsequent findings with EEG).

⁴ For consistency, we repeated the model comparison for the ERP data set with RT normalised data and found that the results were unchanged.

721 Discussion

722 We utilised two separate electrophysiological methods to explore the neurocognitive
723 mechanisms underlying the speed-accuracy tradeoff, a central yet unresolved issue
724 in decision-making research. The model-based behavioural literature suggests that a
725 variation in the decision boundary (or, equivalently, a change in the baseline level)
726 explains the SAT (Brown and Heathcote, 2008; Smith and Ratcliff, 2004; Usher and
727 McClelland, 2001), but recent neural evidence has not supported this claim,
728 suggesting more widespread changes (Hanks et al., 2014; Heitz and Schall, 2012,
729 2013; Murphy et al., 2016). To resolve this paradox, we hypothesised that the SAT
730 may result from changes which are mathematically equivalent to a modulation of the
731 decision boundary, but which are implemented physiologically through global
732 changes in neural activity akin to turning up the gain in the brain. We recorded
733 neurodynamic substrates of decision-making during a motion discrimination task with
734 two difficulty levels and under instructions to focus on either response speed or
735 accuracy. The resulting data converged to favour the predictions made by a forced-
736 excursion model variant in which the SAT is implemented by adjusting both the
737 signal (i.e. accumulation rates v) and noise (i.e. noise parameters S_z and σ) affecting
738 accumulation-related neural activity.

739 Although our main interest was the SAT, we included a difficulty manipulation as a
740 “sanity test” regarding the validity of our neurodynamic decision correlates. The
741 impact of difficulty on evidence accumulation has been demonstrated previously,
742 with both sequential sampling models and proposed neural correlates of
743 accumulation displaying steeper build-up rates in easier decisions (Kelly and
744 O’Connell, 2013; Mulder et al., 2014; Ratcliff and McKoon, 2008; Roitman and

745 Shadlen, 2002). Accordingly, we found that faster and more accurate responses in
746 easy trials were explained by higher accumulation rates in both experiments. These
747 patterns were observed in both neural signals and their simulated accumulation
748 profiles and, consistently with previous studies (Hadar et al., 2016; O'Connell et al.,
749 2012), support the role of MEP and CPP signals as neural correlates of the decision
750 variable, with corticospinal excitability likely receiving a time-lagged but continuous
751 input from CPP/decision-generating regions.

752 Like the difficulty manipulation, SAT instructions also resulted in the expected
753 behavioural changes, with faster and more error prone responses under speed
754 instructions. In line with many previous studies (Brown and Heathcote, 2008; Heitz,
755 2014; Ratcliff and McKoon, 2008; Usher and McClelland, 2001), our free-excursion
756 race model accounted for behavioural effects of the SAT, primarily by varying the
757 amount of accumulated evidence required to make a decision. However, since
758 recent studies exploring neural correlates of decision-making have challenged this
759 implementation of the SAT (Hanks et al., 2014; Heitz and Schall, 2012, 2013;
760 Murphy et al., 2016), we used a forced-excursion variant which models a global gain
761 modulation by adjusting the parameters of the free-excursion race model so that the
762 boundary was equal across SAT conditions, thus transferring the estimated
763 difference between response bounds onto all other parameters affecting
764 accumulation. In other words, a fixed boundary between SAT conditions was made
765 mathematically equivalent to the free-excursion model by assuming different
766 underlying mechanisms, with changes between SAT conditions explained not by
767 boundary differences, but by differences between virtually all other parameters,
768 modelling a global shift in decision-related brain activity.

769 When we compared predicted accumulation profiles from both the free and the
770 forced-excursion model variants to our neural data, a fixed boundary provided
771 significantly better degrees of correspondence between them (we avoid the term
772 “goodness of fit” here, because predictions were based on RT data, with little
773 adjustment required to capture neurodynamic trends). We should, however, offer the
774 caveat that the statistical basis of this result is unconventional. By utilising
775 permutation tests on pooled data, we compared against sampling distributions
776 derived from the population of all possible trials from our particular set of
777 participants, rather than the population of all possible participants. However,
778 generalisations to an even less representative population (e.g. all neurons of a given
779 type within a single monkey) are commonplace in neuroscience. Furthermore, there
780 are several additional observations that support our conclusion that the forced-
781 excursion model variant was best. In both model and data, the stimulus-locked
782 profiles displayed a slope difference between easy and hard trials and no difference
783 between speed and accuracy trials. Importantly, in the response-locked model
784 predictions, the terminal amplitude differences between SAT conditions were
785 reduced compared to the predictions retaining a free excursion, better resembling
786 the neural signals. These findings support the hypothesis that differences induced by
787 SAT instructions are explained by a global modulation of activity rather than by
788 varying a single specific parameter/process.

789 Previous attempts to explain the SAT in the absence of variation in the decision
790 boundary have done so by incorporating an urgency signal, i.e. an evidence-
791 independent signal, which over time pushes the accumulation process towards a
792 boundary (Cisek et al., 2009; Hawkins et al., 2015; Thura et al., 2012). This
793 integration of urgency is not dissimilar to our suggestion of an amplified

794 accumulation process. Both approaches avoid a variation in response boundary by
 795 boosting accumulation in hasty decisions, and make broadly analogous predictions
 796 regarding the SAT's impact on accumulation profiles.

797 However, urgency models do differ mathematically from our forced-excursion model.
 798 While the former assume the addition of an independent and *growing* signal, i.e. a
 799 *time-varying* process, the latter is obtained by an adjustment of parameters derived
 800 from the more established free-excursion model, implying a *time-invariant* intrinsic
 801 amplification of the accumulation process induced by global changes of the system.
 802 To expand on this distinction (with the important caveat that the urgency has been
 803 implemented in different ways by different authors) – urgency may be implemented
 804 as the addition of an evidence-independent signal at each time step, with this signal
 805 growing over time (e.g. Hanks et al., 2014), or as the multiplication of evidence by
 806 such a signal (e.g. Ditterich, 2006) in which case accumulation noise is also subject
 807 to this time-varying gain. In the latter approach, the integration of evidence over time
 808 may additionally be deliberately downplayed via (very) leaky integration (e.g. Cisek
 809 et al., 2009). By contrast, our modelling instead captured the SAT by amplifying both
 810 signal and noise in a constant manner *throughout the decision* (with noise even
 811 amplified prior to the onset of the imperative stimulus, via the S_2 parameter). This is
 812 what we mean here by neural gain modulation – the amplification of both signal and
 813 noise in a time-independent manner. Note that the way starting-point noise was
 814 implemented here implies that it effectively conflates mean starting point with start-
 815 point variability (see methods/results). In this sense, our “fixed-excursion”
 816 terminology is a slight misnomer – some part of our model's ability to explain the
 817 SAT in both behavioural and neural data is still dependent on a reduction in

818 excursion, but several other parameters also play a role, and the decision bound is
819 fixed.

820 We wish to note that we are in no sense hostile to the concept of urgency. In fact, we
821 tested urgency models as an additional exploratory analysis, but opted not to include
822 these results for reasons of brevity and clarity.⁵ Indeed, we find the concept of
823 “urgency” to be a useful one that somewhat overlaps our “neural gain” hypothesis
824 and finds support in the neuroscientific literature (e.g. Thura and Cisek, 2017).
825 Therefore, we do not claim that our model is better supported than urgency models,
826 either here or in general. However, since a number of studies evaluating the concept
827 of an urgency signal have been unable to support it, suggesting instead that
828 standard sequential sampling models can fully account for all behavioural data (Balci
829 et al., 2011; Hawkins et al., 2015; Karsilar et al., 2014), we propose that forced-
830 excursion model variants should at least be considered as an appropriate alternative
831 to urgency signals, reconciling decades of model-based support for decision
832 boundary variation with recent neural evidence.

833 Although we have argued that the simulated accumulation profiles of the forced-
834 excursion model closely resemble both of our neural signals, supporting the notion of
835 a global modulation of activity as the underlying mechanism explaining the SAT,
836 there are nonetheless some differences between the empirical and simulated
837 profiles. However, any model is a simplified approximation of the true neurocognitive
838 mechanisms and is unlikely to perfectly simulate any given process. This is
839 particularly the case for neural signals which inherently have a low signal-to-noise-

⁵ We implemented two kinds of urgency model, with a linear urgency signal proving more successful. This model was about as good as those we present here when fitting our behavioural data (it provided a better fit in the EEG experiment, but a worse one in the TMS experiment). For neurodynamic data, it performed very similarly to our forced-excursion model in the EEG experiment. Its ability to capture these data in the TMS experiment lay approximately mid-way between our forced and free-excursion classic models, but did not differ significantly from either one.

ratio, such as ERPs and in particular the MEP signal. Somewhat limited signal quality is however typical for experiments of this nature (Hadar et al., 2016; O'Connell et al., 2012), and we used large numbers of trials in both experiments, producing demonstrably interpretable neural signals. We would argue that the correspondence between model predictions and neural data, both here and elsewhere, is remarkable, given a class of models originally conceived to have a largely behavioural scope (Luce, 1986).

All neuroscientific methods have limitations. For example, our MEP signal is derived from a technique that both records and perturbs neural activity, with implications that are difficult to precisely predict (Hadar et al., 2016). However, methodological triangulation is an established approach to building a convincing body of evidence. Here, we obtained converging evidence from two fundamentally different signals, as both corticospinal excitability and a parietal ERP displayed qualitatively similar findings. While there were small practical differences between the experiments (e.g. one vs. multiple sessions, bilateral vs. unilateral responses), these are unlikely to qualitatively alter the accumulation process, and we have matched the simulation of model predictions to the processing of each neural signal to further reduce the impact of methodological differences on our interpretation. Although the suggestion that these signals represent decision accumulation is recent, both signals were modulated by the difficulty manipulation, supporting this account. Furthermore, previous research using more established neural correlates of decision-making in non-human primates has shown similar findings, suggesting widespread changes in activity when the SAT is manipulated (Hanks et al., 2014; Heitz and Schall, 2012, 2013). Collectively, we believe these neural findings warrant adjusting even a well-

864 established model (by rescaling its parameters) given that the adjustment is purely
865 conceptual and does not affect the behavioural fit.

866 A final potential concern relates to our decision to fit models to pooled data, i.e. at
867 the group, rather than individual, level. Such collation may give rise to distorted RT
868 distributions relative to the shape of underlying individual distributions. However,
869 where comparisons have been made between the mean of sequential sampling
870 model parameters derived from individual fits, and the same parameters derived
871 from a single group fit, they have tended to suggest that the group fitting approach is
872 not particularly problematic (e.g. Ratcliff et al., 2003, 2004). The procedure has been
873 used in several recent papers (e.g. Dmochowski and Norcia, 2015; Twomey et al.,
874 2015).

875 In conclusion, we set out to explore the neural mechanisms of the SAT by examining
876 two neural correlates of the decision variable, an MEP signal reflecting corticospinal
877 excitability and a parietal ERP component known as the CPP. The SAT is typically
878 explained in sequential sampling models as a variation of the decision boundary.
879 Here, we tested whether this variation is visible in neural activity or if it might instead
880 be implemented through a mathematically equivalent gain change in neural activity.
881 Our decision-related neural activity, independently sourced from two brain networks,
882 resembled the accumulation profiles predicted by a forced-excursion model variant in
883 which the boundary differences are transferred onto other decision parameters.
884 Consistent with previous studies, our results therefore indicate that the SAT is
885 implemented by global changes of neural activity, but that this conceptually important
886 outcome does not necessarily invalidate traditional modelling approaches.

887

888 **References**

- 889 Akaike H (1977) On entropy maximization principle. In: Applications of Statistics
890 (Krishnaiah PR, ed), pp27–41). Amsterdam.
- 891 Balci F, Freestone D, Simen P, deSouza L, Cohen JD, Holmes P (2011) Optimal
892 Temporal Risk Assessment. *Front Integr Neurosci* 5:1–15.
893 <http://doi.org/10.3389/fnint.2011.00056>
- 894 Barr DJ, Levy R, Scheepers C, Tily HJ (2014) Random effects structure for
895 confirmatory hypothesis testing: Keep it maximal. *J Mem Lang* 68:1–43.
896 <http://doi.org/10.1016/j.jml.2012.11.001>
- 897 Bestmann S, Harrison LM, Blankenburg F, Mars RB, Haggard P, Friston KJ,
898 Rothwell JC (2008) Influence of Uncertainty and Surprise on Human
899 Corticospinal Excitability during Preparation for Action. *Curr Biol* 18:775–780.
900 <http://doi.org/10.1016/j.cub.2008.04.051>
- 901 Blair RC, Karniski W (1993) An alternative method for significance testing of
902 waveform difference potentials. *Psychophysiology* 30:518–524.
- 903 Bogacz R, Brown E, Moehlis J, Holmes P, Cohen JD (2006) The physics of optimal
904 decision making: A formal analysis of models of performance in two-alternative
905 forced-choice tasks. *Psychol Rev* 113:700–765. [http://doi.org/10.1037/0033-](http://doi.org/10.1037/0033-295X.113.4.700)
906 [295X.113.4.700](http://doi.org/10.1037/0033-295X.113.4.700)
- 907 Brainard DH (1997) The Psychophysics Toolbox. *Spatial Vision* 10:433–436.
908 <http://doi.org/10.1163/156856897X00357>

- 909 Brown SD, Heathcote A (2008) The simplest complete model of choice response
 910 time: Linear ballistic accumulation. *Cognitive Psychol* 57:153–178.
 911 <http://doi.org/10.1016/j.cogpsych.2007.12.002>
- 912 Burnham KP, Anderson DR (2004) Multimodel Inference Understanding AIC and BIC
 913 in Model Selection. *Sociol Method Res* 33:261–304.
 914 <http://doi.org/10.1177/0049124104268644>
- 915 Chittka L, Dyer AG, Bock F, Dornhaus A (2003) Psychophysics: Bees trade off
 916 foraging speed for accuracy. *Nature* 424:388–388.
 917 <http://doi.org/10.1038/424388a>
- 918 Cisek P, Puskas GA, El-Murr S (2009) Decisions in Changing Conditions: The
 919 Urgency-Gating Model. *J Neurosci* 29:11560–11571.
 920 <http://doi.org/10.1523/JNEUROSCI.1844-09.2009>
- 921 Delorme A, Makeig S (2004) EEGLAB: An open source toolbox for analysis of
 922 single-trial EEG dynamics including independent component analysis. *J*
 923 *Neurosci Meth* 134:9–21. <http://doi.org/10.1016/j.jneumeth.2003.10.009>
- 924 Ditterich J (2006) Evidence for time-variant decision making. *Eur J Neurosci*,
 925 24:3628–41. <http://doi.org/https://doi.org/10.1111/j.1460-9568.2006.05221.x>
- 926 Dmochowski JP, Norcia AM (2015) Cortical components of reaction-time during
 927 perceptual decisions in humans. *PLoS ONE* 10:1–18.
 928 <http://doi.org/10.1371/journal.pone.0143339>
- 929 Donkin C, Brown SD, Heathcote A (2009) The overconstraint of response time
 930 models: Rethinking the scaling problem. *Psychon B Rev* 16:1129–1135.
 931 <http://doi.org/10.3758/PBR.16.6.1129>

- 932 Donkin C, Brown S, Heathcote A, Wagenmakers E (2011) Diffusion versus linear
 933 ballistic accumulation: different models but the same conclusions about
 934 psychological processes? *Psychon B Rev* 18:61–69.
 935 <http://doi.org/10.3758/s13423-010-0022-4>
- 936 Donkin C, Heathcote A, Brown S (2009) Is the Linear Ballistic Accumulator Model
 937 Really the Simplest Model of Choice Response Times: A Bayesian Model
 938 Complexity Analysis. In 9th International Conference on Cognitive Modeling—
 939 ICCM2009 (Manchester, UK).
- 940 Donner TH, Siegel M, Fries P, Engel AK (2009) Buildup of Choice-Predictive Activity
 941 in Human Motor Cortex during Perceptual Decision Making. *Curr Biol* 19:1581–
 942 1585. <http://doi.org/10.1016/j.cub.2009.07.066>
- 943 Duque J, Greenhouse I, Labruna L, Ivry RB (2017) Physiological Markers of Motor
 944 Inhibition during Human Behavior. *Trends Neurosci* 40:219–236.
 945 <http://doi.org/10.1016/j.tins.2017.02.006>
- 946 Duque J, Lew D, Mazzocchio R, Olivier E, Ivry RB (2010) Evidence for Two
 947 Concurrent Inhibitory Mechanisms during Response Preparation. *J Neurosci*
 948 30:3793–3802. <http://doi.org/10.1523/JNEUROSCI.5722-09.2010>
- 949 Evans NJ, Hawkins GE, Boehm U, Wagenmakers EJ, Brown SD (2017) The
 950 computations that support simple decision-making: A comparison between the
 951 diffusion and urgency-gating models. *Sci Rep* 7:1–13.
 952 <http://doi.org/10.1038/s41598-017-16694-7>
- 953 Gold JI, Shadlen MN (2000) Representation of a perceptual decision in developing
 954 oculomotor commands. *Nature* 404:390–394. <http://doi.org/10.1038/35006062>

- 955 Groppe DM, Urbach TP, Kutas M (2011) Mass univariate analysis of event-related
 956 brain potentials/fields I: A critical tutorial review. *Psychophysiology* 48:1711–
 957 1725. <http://doi.org/10.1111/j.1469-8986.2011.01273.x>
- 958 Hadar A, Rowe P, Di Costa S, Jones A, Yarrow K (2016) Motor-evoked potentials
 959 reveal a motor-cortical readout of evidence accumulation for sensorimotor
 960 decisions. *Psychophysiology* 53:1721-1731.doi: 10.1111/psyp.12737
- 961 Hanks TD, Kiani R, Shadlen MN (2014) A neural mechanism of speed-accuracy
 962 tradeoff in macaque area LIP. *eLife* 27:1–17. <http://doi.org/10.7554/eLife.02260>
- 963 Hawkins GE, Forstmann BU, Wagenmakers EJ, Ratcliff R, Brown SD (2015)
 964 Revisiting the evidence for collapsing boundaries and urgency signals in
 965 perceptual decision-making. *J Neurosci* 35:2476–84.
 966 <http://doi.org/10.1523/JNEUROSCI.2410-14.2015>
- 967 Hawkins GE, Wagenmakers EJ, Ratcliff R, Brown SD (2015) Discriminating
 968 evidence accumulation from urgency signals in speeded decision making. *J*
 969 *Neurophysiol* 114:40-47. <http://doi.org/10.1152/jn.00088.2015>
- 970 Heathcote A, Brown S, Mewhort DJK (2002) Quantile maximum likelihood estimation
 971 of response time distributions. *Psychon B Rev* 9:1–31.
 972 <http://doi.org/10.3758/BF03196299>
- 973 Heitz RP (2014) The speed-accuracy tradeoff: History, physiology, methodology, and
 974 behavior. *Front Neurosci* 8:1–19. <http://doi.org/10.3389/fnins.2014.00150>
- 975 Heitz RP, Schall JD (2012) Neural Mechanisms of Speed-Accuracy Tradeoff. *Neuron*
 976 76:616–628. <http://doi.org/10.1016/j.neuron.2012.08.030>

- 977 Heitz RP, Schall JD (2013) Neural chronometry and coherency across speed-
 978 accuracy demands reveal lack of homomorphism between computational and
 979 neural mechanisms of evidence accumulation. *Philos T Roy Soc B*
 980 368:20130071. <http://doi.org/10.1098/rstb.2013.0071>
- 981 Hick WE (1952) On the rate of gain of information. *Q J Exp Psychol* 4:11–26.
 982 [http://doi.org/10.1016/0022-0965\(78\)90002-4](http://doi.org/10.1016/0022-0965(78)90002-4)
- 983 Ivanoff J, Branning P, Marois R (2008) fMRI evidence for a dual process account of
 984 the speed-accuracy tradeoff in decision-making. *PLoS ONE* 3.
 985 <http://doi.org/10.1371/journal.pone.0002635>
- 986 Karsilar H, Simen P, Papadakis S, Balci F (2014) Speed accuracy trade-off under
 987 response deadlines. *Front Neurosci* 8:1–18.
 988 <http://doi.org/10.3389/fnins.2014.00248>
- 989 Kayser J, Tenke CE (2006) Principal components analysis of Laplacian waveforms
 990 as a generic method for identifying ERP generator patterns: II. Adequacy of low-
 991 density estimates. *Clin Neurophysiol* 117:369–380.
 992 <http://doi.org/10.1016/j.clinph.2005.08.033>
- 993 Kelly SP, O'Connell RG (2013) Internal and external influences on the rate of
 994 sensory evidence accumulation in the human brain. *J Neurosci* 33:19434–
 995 19441. <http://doi.org/10.1523/JNEUROSCI.3355-13.2013>
- 996 Klein-Flugge MC, Bestmann S (2012) Time-Dependent Changes in Human
 997 Corticospinal Excitability Reveal Value-Based Competition for Action during
 998 Decision Processing. *J Neurosci* 32:8373–8382.
 999 <http://doi.org/10.1523/JNEUROSCI.0270-12.2012>

- 1000 Kleiner M, Brainard DH, Pelli DG, Broussard C, Wolf T, Niehorster D (2007) What's
1001 new in Psychtoolbox-3? Perception 36. <http://doi.org/10.1068/v070821>
- 1002 Laberge D (1962) A recruitment theory of simple behavior. Psychometrika 27:375–
1003 396.
- 1004 Lagarias JC, Reeds JA, Wright MH, Wright PE (1998) Convergence Properties of the
1005 Nelder-Mead Simplex Method in Low Dimensions. SIAM J Optimiz 9:112–147.
1006 <http://doi.org/10.1137/S1052623496303470>
- 1007 Luce RD (1986) Response Times: Their Role in Inferring Elementary Mental
1008 Organization. New York: Oxford University Press.
- 1009 Milosavljevic M, Malmaud J, Huth A (2010) The Drift Diffusion Model can account for
1010 the accuracy and reaction time of value-based choices under high and low time
1011 pressure. Judgem Decis Mak 5:437–449. <http://doi.org/10.2139/ssrn.1901533>
- 1012 Mulder MJ, van Maanen L, Forstmann BU (2014) Perceptual decision neurosciences
1013 - a model-based review. Neuroscience 277:872–884.
1014 <http://doi.org/10.1016/j.neuroscience.2014.07.031>
- 1015 Murphy PR, Boonstra E, Nieuwenhuis S (2016) Global gain modulation generates
1016 time-dependent urgency during perceptual choice in humans. Nat Commun
1017 7:13526. <http://doi.org/10.1038/ncomms13526>
- 1018 Nichols TE, Holmes AP (2001) Nonparametric Permutation Tests for {PET}
1019 functional Neuroimaging Experiments: A Primer with examples. Hum Brain
1020 Mapp 15:1–25. <http://doi.org/10.1002/hbm.1058>

- 1021 O'Connell RG, Dockree PM, Kelly SP (2012) A supramodal accumulation-to-bound
 1022 signal that determines perceptual decisions in humans. *Nat Neurosci* 15:1729–
 1023 35. <http://doi.org/10.1038/nn.3248>
- 1024 Pelli DG (1997) The VideoToolbox software for visual psychophysics: transforming
 1025 numbers into movies. *Spatial Vision*. <http://doi.org/10.1163/156856897X00366>
- 1026 Price KV, Storn RM, Jouni LA (2005). *Differential Evolution: A Practical Approach to*
 1027 *Global Optimization*. Heidelberg: Springer Berlin Heidelberg.
 1028 <http://doi.org/10.1038/155531c0>
- 1029 Ratcliff R (1978). A theory of memory retrieval. *Psychol Rev* 85:59–108.
 1030 <http://doi.org/10.1037/0033-295X.85.2.59>
- 1031 Ratcliff R, McKoon G (2008) The diffusion decision model: theory and data for two-
 1032 choice decision tasks. *Neural Comput* 20:873–922.
 1033 <http://doi.org/10.1162/neco.2008.12-06-420>
- 1034 Ratcliff R, Rouder JN (1998) Modeling Response Times for Two-Choice Decisions.
 1035 *Psychol Sci* 9:347–356.
- 1036 Ratcliff R, Thapar A, McKoon G (2003) A diffusion model analysis of the effects of
 1037 aging on brightness discrimination. *Percept Psychophys* 65:523–35.
 1038 <http://doi.org/10.3758/BF03194580>
- 1039 Ratcliff R, Thapar A, McKoon G (2004) A diffusion model analysis of the effects of
 1040 aging on recognition memory. *J Mem Lang* 50:408–424.
 1041 <http://doi.org/10.1016/j.jml.2003.11.002>

- 1042 Resulaj A, Kiani R, Wolpert DM, Shadlen MN (2009) Changes of mind in decision-
 1043 making. *Nature* 461:263–266. <http://doi.org/10.1038/nature08275>
- 1044 Roitman JD, Shadlen MN (2002) Response of neurons in the lateral intraparietal
 1045 area during a combined visual discrimination reaction time task. *J Neurosci*
 1046 22:9475–9489. [http://doi.org/10.1016/S0377-2217\(02\)00363-6](http://doi.org/10.1016/S0377-2217(02)00363-6)
- 1047 Shadlen MN, Newsome WT (1996) Motion perception: seeing and deciding. *P Natl*
 1048 *Acad Sci USA* 93:628–633. <http://doi.org/10.1073/pnas.93.2.628>
- 1049 Shadlen MN, Newsome WT (2001) Neural Basis of a Perceptual Decision in the
 1050 Parietal Cortex (Area LIP) of the Rhesus Monkey. *J Neurophysiol* 86:1916–
 1051 1936.
- 1052 Smith PL, Ratcliff R (2004) Psychology and neurobiology of simple decisions. *Trends*
 1053 *Neurosci* 27:161–168. <http://doi.org/10.1016/j.tins.2004.01.006>
- 1054 Thura D, Beauregard-Racine J, Fradet CW, Cisek P (2012) Decision making by
 1055 urgency gating: theory and experimental support. *J Neurophysiol* 108:2912–
 1056 2930. <http://doi.org/10.1152/jn.01071.2011>
- 1057 Thura D, Cisek P (2017) The Basal Ganglia Do Not Select Reach Targets but
 1058 Control the Urgency of Commitment. *Neuron* 95:1160–1170.
 1059 <http://doi.org/10.1016/j.neuron.2017.07.039>
- 1060 Twomey DM, Kelly SP, O'Connell RG (2016) Abstract and Effector-Selective
 1061 Decision Signals Exhibit Qualitatively Distinct Dynamics before Delayed
 1062 Perceptual Reports. *J Neurosci* 36:7346–7352.
 1063 <http://doi.org/10.1523/JNEUROSCI.4162-15.2016>

- 1064 Twomey DM, Murphy PR, Kelly SP, O'Connell RG (2015) The classic P300 encodes
1065 a build-to-threshold decision variable. *Eur J Neurosci* 42:1636–1643.
1066 <http://doi.org/10.1111/ejn.12936>
- 1067 Usher M, McClelland JL (2001) The time course of perceptual choice: The leaky,
1068 competing accumulator model. *Psychol Rev* 108:550–592.
1069 <http://doi.org/10.1037/0033-295X.108.3.550>
- 1070 Vickers D (1970) Evidence for an Accumulator Model of Psychophysical
1071 Discrimination. *Ergonomics* 13:37–58.
1072 <http://doi.org/https://doi.org/10.1080/001401370008931117>
- 1073 Watson AP, Pelli DG (1983) QUEST: A Bayesian adaptive psychometric method.
1074 *Percept Psychophys* 33:113–120.
- 1075 Wickelgren WA (1977) Speed-Accuracy Tradeoff and Information Processing
1076 Dynamics. *Acta Psychol* 41:67–85.
- 1077

1078 **Table Legends**

1079 Table 1: Model Comparison: BIC and AIC values for each model and each
1080 experiment (best BIC and AIC values in bold).The terms "fixed" and "free" here
1081 relate specifically to changes across speed/accuracy instructions, as accumulation
1082 rate (V) was always free to vary between difficulty conditions.

1083

1084 Table 2: Estimated parameter values for the best-supported model (Model 2) when
1085 expressed with both free and forced-excursion in both experiments. The response
1086 boundary A in the 'accuracy' condition was set to 1 as a scaling parameter.
1087 Parameters are not comparable across experiments, as the TMS fit is to data
1088 normalised to the median RT of each participant.

Figure Captions

Figure 1: TMS experiment procedure: a) random dot motion task: after a fixation cross and a period of random motion, coherent motion (here: upward, coherence 70%) is displayed for 2000 ms or until response (the same task was used in the EEG experiment); b) response setup in TMS experiment: Participants held one button (up) between their thumb and index finger (pinch) and one in the palm of their hand (down), attached to a cylinder (grasp); EMG electrodes were placed on the ADM and FDI; c) example EMG traces from a single trial (here, a hard speed trial, where the responding muscle is the FDI and the non-responding muscle is the ADM); d) To create model predictions which are comparable to MEP data, accumulation values from both the correct accumulator (corresponding to the responding muscle) and the incorrect accumulator (corresponding to the non-responding muscle) are sampled at simulated TMS times; e) Illustrative real MEP amplitudes (from the speed/easy condition) collated from all participants; f) MEPs and simulations (not shown) are then z-scored per muscle, participant, and session (note that latencies were normalised by the median, not maximum, EMG RT for each participant); g) real and simulated continuous signals can be created for each muscle (responding, non-responding), using a Gaussian smoothing kernel; h) however, to remove non-specific processes, the same smoothing is applied to the difference between simultaneously recorded MEPs (responding minus non-responding).

1110 Figure 2: Behavioural results for both the TMS experiment (a) and the EEG
1111 experiment (b): reaction time (left) and accuracy scores (right) for each condition.
1112 Top left panel shows both EMG RT (bars) and button RT (dashed lines). Error bars
1113 indicate 95% Confidence Interval. ** indicates $p < .001$.
1114

1115 Figure 3: Neural and modelling results: Top: neural data; Bottom: model comparison;
1116 Left: TMS experiment; Right: EEG experiment; a) stimulus-locked (left) and
1117 response-locked (right) MEP signal for each condition. Each panel shows both the
1118 MEP signal associated with the responding muscle (dark) and the non-responding
1119 muscle (light). Shaded areas indicate 95% confidence intervals; b) CPP: stimulus-
1120 locked (left) and response-locked (right) CPP waveform for each condition. The
1121 bottom right of the panel shows the topography of the ERP, averaged over the
1122 stimulus-locked time interval of 0 to 1000 ms. Electrodes used to generate CPP
1123 waveforms are highlighted; c) stimulus-locked (left) and response-locked (right)
1124 MEP-average signal (responding minus non-responding muscle); d) stimulus-locked
1125 (left) and response-locked (right) model predictions made by the free-excursion
1126 variant of the best-supported model; e) stimulus-locked (left) and response-locked
1127 (right) model predictions made by the forced-excursion variant of the best-supported
1128 model; f) stimulus-locked (left) and response-locked (right) CPP; note that the CPP
1129 here is a pooled average rather than a grand average and therefore differs from b.
1130 Additionally, the waveform has been low-pass filtered with a cut-off of 5 Hz to assist
1131 comparison with model predictions; f) stimulus-locked (left) and response-locked
1132 (right) model predictions (correct and incorrect accumulator summed) made by the
1133 free-excursion variant of the best-supported model; g) stimulus-locked (left) and
1134 response-locked (right) model predictions (correct and incorrect accumulator
1135 summed) made by the forced-excursion variant of the best-supported model.

1136

1137

1138

1139 Figure 4: Model fit for the TMS experiment (a) and the EEG experiment (b): quantiles
1140 estimated from behavioural data (circles) and Model 2 simulations (crosses and
1141 lines) for easy (top) and hard (bottom) decisions. For each condition, correct (thick)
1142 and incorrect (thin) quantiles are displayed separately. Note that the model fit is
1143 identical for the forced-excursion and the standard free-excursion race model.

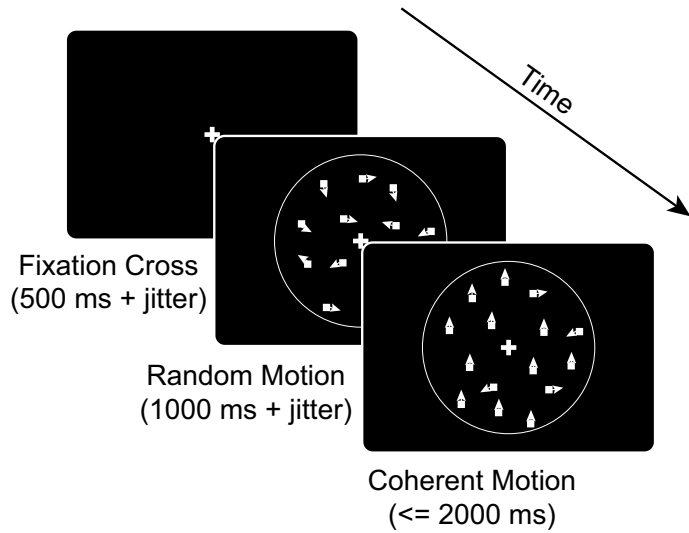
1144

1145

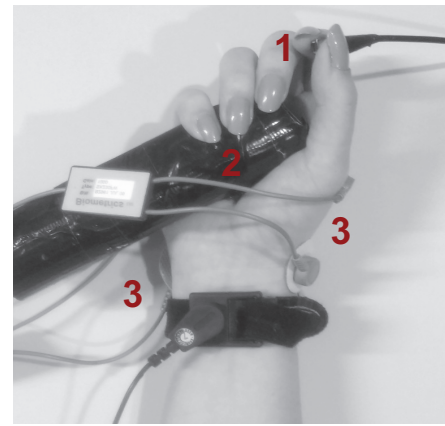
Model Number	A	S _z	V _{correct}	V _{incorrect}	T _{or}	S _{ter}	σ	Number of parameters	TMS		EEG	
									Experiment		Experiment	
									AIC	BIC	AIC	BIC
Model 1	free	fixed	fixed	fixed	fixed	fixed	fixed	9	44,868	44,933	62,398	62,466
Model 2	free	free	fixed	fixed	fixed	fixed	fixed	10	44,859	44,932	62,389	62,464
Model 3	free	fixed	fixed	fixed	free	fixed	fixed	10	44,865	44,937	62,404	62,479

Parameters	TMS Experiment				EEG Experiment			
	Free-excursion		Forced-excursion		Free-excursion		Forced-excursion	
	accuracy	speed	accuracy	speed	accuracy	speed	accuracy	speed
S_z	0.447	0.523	0.447	0.586	0.319	0.541	0.319	0.664
A	1	0.893	1		1	0.815	1	
T_{er}	0.382		0.382		0.257		0.257	
S_{Ter}	0.374		0.374		0.229		0.229	
σ^2	0.499		0.499	0.558	0.785		0.785	0.964
$V_{correct}$	<i>easy</i>	1.280	1.28	1.433	2.475		2.475	3.038
	<i>hard</i>	0.634	0.634	0.710	1.350		1.350	1.656
$V_{incorrect}$	<i>easy</i>	0.098	0.098	0.109	0.253		0.253	0.310
	<i>hard</i>	0.004	0.004	0.005	0.054		0.054	0.066

a) Random dot motion task

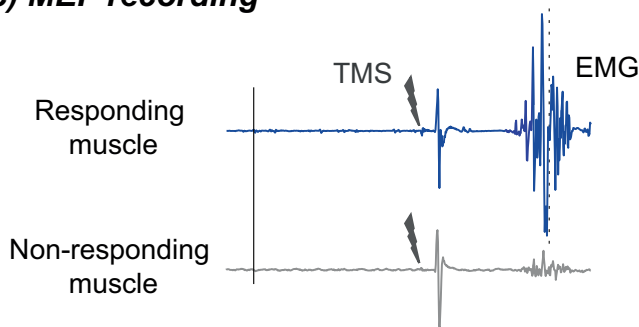


b) Response/EMG setup

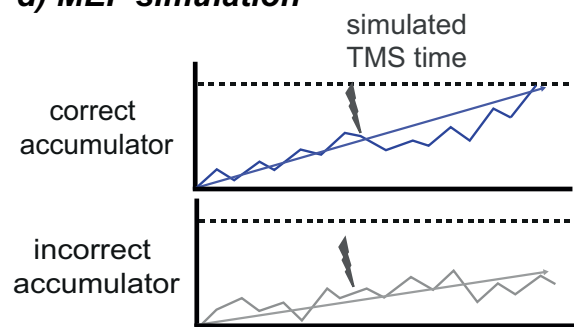


- 1 'Pinch' response button
- 2 'Grasp' response button
- 3 EMG electrodes

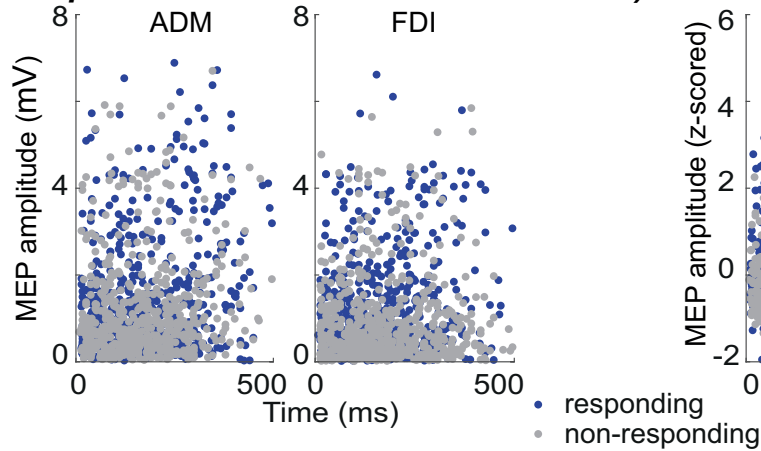
c) MEP recording



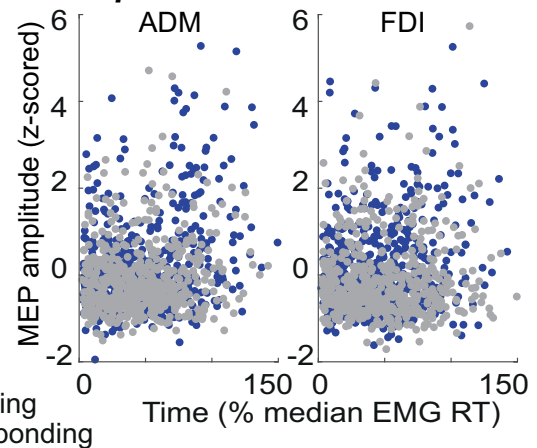
d) MEP simulation



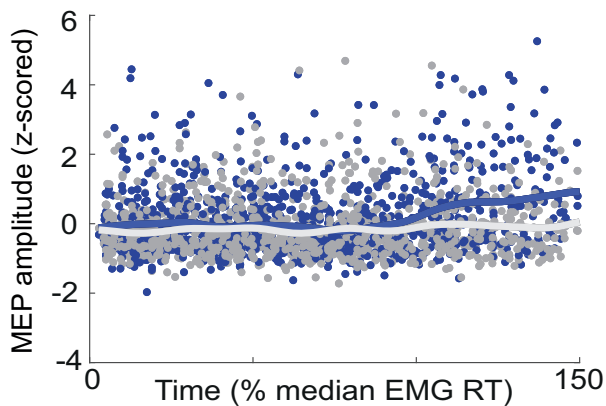
e) MEP amplitudes: raw data



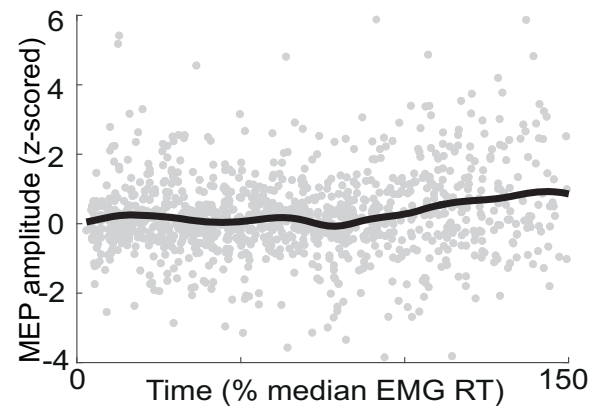
f) MEP amplitudes: normalised



g) MEP smoothing

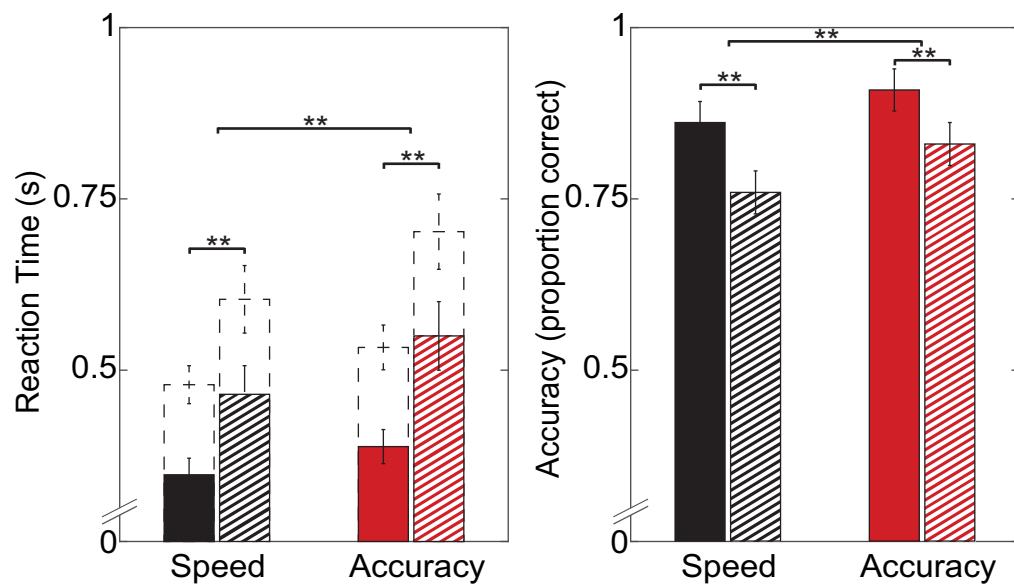


h) MEP subtraction

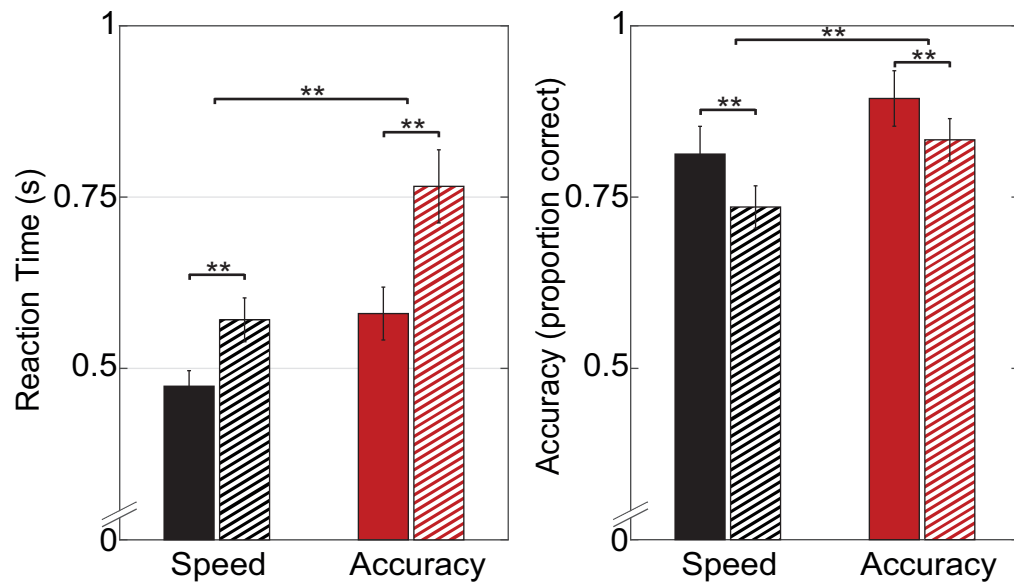


a) TMS Experiment

Speed Easy Speed Hard
 Accuracy Easy Accuracy Hard

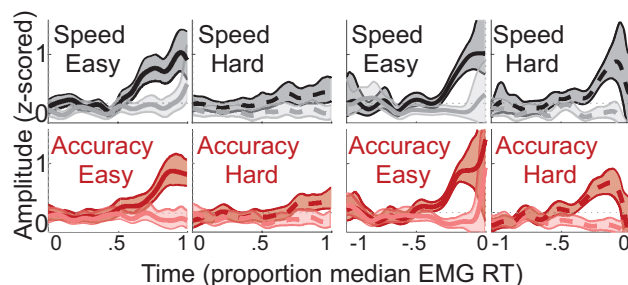


b) EEG Experiment



TMS Experiment

a) MEP data



Responding Muscle

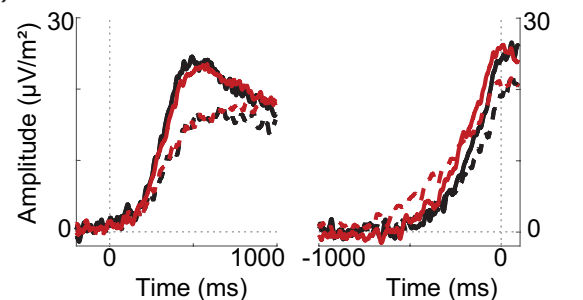
— Speed Easy
- - Speed Hard
— Accuracy Easy
- - Accuracy Hard

Non-responding Muscle

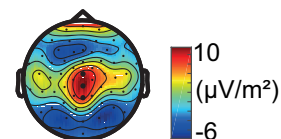
— Speed Easy
- - Speed Hard
— Accuracy Easy
- - Accuracy Hard

EEG Experiment

b) CPP

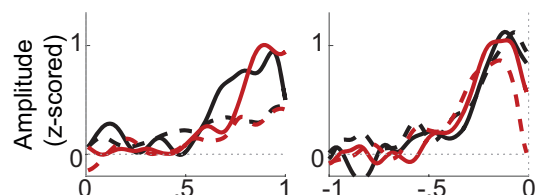


— Speed Easy
- - Speed Hard
— Accuracy Easy
- - Accuracy Hard

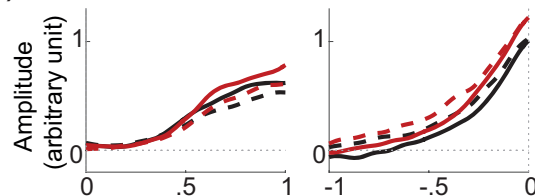


TMS Data & Model Prediction

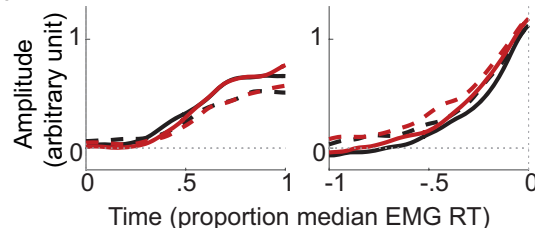
c) MEP Difference



d) Free-Excursion Model



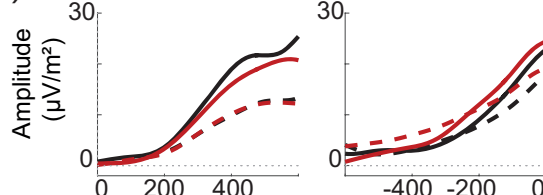
e) Forced-Excursion Model



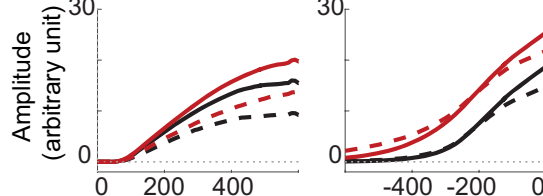
— Speed Easy — Accuracy Easy
- - Speed Hard - - Accuracy Hard

EEG Data & Model Prediction

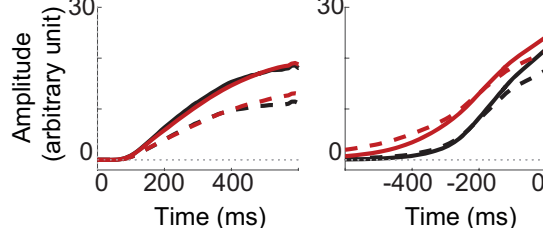
f) CPP



g) Free-Excursion Model



h) Forced-Excursion Model



a) TMS Experiment

b) EEG Experiment

